Theoretical Chemistry Accounts (2018) 137:12
https://doi.org/10.1007/s00214-017-2185-9

REGULAR ARTICLE

# $TiO_2$ nanotubes sensitized with CdSe quantum dots

**Roger Nadler**[1] · **Javier Fernández Sanz**[1]

Received: 20 September 2017 / Accepted: 19 December 2017 / Published online: 4 January 2018


**Abstract**
Quantum dot-sensitized solar cells (QDSSCs) are becoming a viable alternative in the market of the third-generation solar cells. Replacing conventional $TiO_2$ or ZnO thin films with anatase $TiO_2$ nanotubes (NTs) leads to a faster charge separation of the excited electron from the quantum dot (QD) to the anode and, consequently, to higher efficiencies. In addition, the adsorption mode of the QDs to the nanotube plays a significant role in the quest for more efficient QDSSCs. We investigate these effects by means of density functional theory (DFT) and real-time time-dependent DFT. Differently sized QDs [$(CdSe)_{13}$ and $(CdSe)_{34}$, bare clusters and saturated with methylamine and *p*-toluidine] are added to different anatase $TiO_2$ nanotubes [NT(0,8), NT(0,12), NT(0,16)]. We considered direct adsorption or linkage via mercaptopropionic acid (MPA). First, the nanotube diameter does not affect the electronic absorption spectra. When the QDs are linked with MPA, we find that the absorption spectrum resembles that of the single QD. Also, the size of the QD has a significant impact on the absorption spectrum and it can happen that the conduction band (CB) of an unsaturated QD lies below that of the nanotube. Saturation of the QD's surface pushes the CB up again. Furthermore, aromatic ligands increase the first absorption peak maximum to higher energies.

**Keywords** Titanium oxide nanotubes · Solar cells · Quantum dots · Computational modeling · Real-time time-dependent DFT (RT-TDDFT)

## 1 Introduction

Semiconductor nanostructures of metal chalcogenides like CdSe, CdS, PbSe and others have become promising candidates to further increase availability and efficiency of the third-generation solar cells [1]. These so-called quantum dots (QDs) have unique properties like a diameter-dependent absorption spectrum. They are easy to synthesize, and consequently, quantum dot-sensitized solar cells (QDSSCs) that use these nanoclusters are more quickly and cheaply available. The desired wavelength of the absorbed light can be tuned equally as easily, which enhances the efficiency of such solar cells. Furthermore, their usage offers the production of flexible solar cells, similar to dye-sensitized solar cells (DSSCs). The only disadvantage is the lower efficiencies compared to DSSCs (which employ efficiencies of up to 14%): for quantum dot-sensitized solar cells (QDSSCs) that work with liquid electrolytes a power conversion efficiency of 5% has been reported; however, for solid-state QDSSCs, efficiencies arrived at almost 10% [2–6]. Keep in mind that a few years ago efficiencies of hardly 1–2% had been reached.

The crucial process of a QDSSC is the injection of excited electrons generated within the quantum dot (QD) into the conduction band (CB) of the semiconductor electrode. The typical design is that a mesoscopic $TiO_2$ or ZnO film is adsorbed on an optically transparent electrode (OTE). These films do not exceed a thickness of 10 µm. A QD suspension is then added to these films. Different strategies exist to fabricate QDSSCs. Popular methods are drop or spin coating, chemical bath deposition [7, 8], surface ionic layer adsorption and reaction (SILAR) [9], electrophoretic deposition [10, 11] and the bifunctional linker approach [12, 13].

The linker-assisted attachment of QDs to the mesoscopic semiconductor makes use of the fact that the linker has two functional groups. One of them binds to the $TiO_2$ surface, usually via a carboxylic acid group, while the

Published as part of the special collection of articles "In Memoriam of Claudio Zicovich."

✉ Javier Fernández Sanz
sanz@us.es

[1] Departamento de Química Física, Universidad de Sevilla, 41012 Seville, Spain

second substituent coordinates with the metal atoms in the QD. The bifunctional approach has the advantage that it avoids the aggregation of QDs as this leads to a significant decrease in the incident photon-to-current efficiency (IPCE) [13]. It further allows for submonolayer coverage and enhances the photostability of the QDs [14]. This approach has an important disadvantage, in that the electron transfer (ET) rates are consistently slower as if the QD is adsorbed directly on the semiconductor [15] even with short linker molecules like mercaptopropionic acid (MPA) [16]. Using cysteine as the linker may lead to higher IPCEs [17].

Apart from reports where in DSSCs the dye molecules are adsorbed on $TiO_2$ nanoparticles [18], there exists also work that employed $TiO_2$ nanotubes as the sensitized material [19]. Beyond the fact that some of these $TiO_2$ NTs show negative strain energies [20], such nanostructures have the advantage over nanoparticles that they do not have to transport the photogenerated charge across a three-dimensional structure, which is thought to hamper the efficiency of the electron transfer, but rather they are limited to only one dimension and, therefore, charges are separated much faster. Obviously, the same strategy can be chosen for the preparation of QDSSCs, too. For instance, Li et al. [21] reported that the photocatalytic activity of QD–$TiO_2$ nanotube heterostructures is higher than a pure QD solution or $TiO_2$ nanotubes. Other groups reported such QD–$TiO_2$ nanotube systems also as a possible photovoltaic application [17, 22]. The efficiency of the power conversion is still relatively low; it does not exceed 3% in these reports. Also theoretically, $TiO_2$ nanotubes sensitized with QDs have been the subject of investigation. For instance, a $(CdSe)_2$–$TiO_2$ nanotube system was investigated by Dong et al. [23] by means of hybrid DFT calculations. On the other hand, the different components that constitute the QDSCs (the oxide, linkers, ligands or the counter electrode) and the mechanisms that govern their performance should be deeply evaluated to improve the efficiency of these devices. For instance, the role of capping ligands has been studied to improve the photoluminescence efficiency of the devices [24]. The impact of ligands on the morphology, electronic structure and optical response of CdSe QDs has also been reported theoretically by means of time-dependent DFT (TDDFT) [25–27]. Also, the role of the linker has been examined for a variety of QDs including metal sulfides [12, 28–30].

In the present work, we investigate the impact of QD size, saturation of the QD surface with two different ligand molecules and the type of adsorption of the QD to the nanotube. CdSe is used as the nanocluster material while differently sized anatase $TiO_2$ nanotubes act as the electrode. Optical spectra obtained with the real-time time-dependent density functional theory (RT-TDDFT) methodology are compared to partial density of states plots of the atomic orbitals involved in the lowest lying electron excitation, i.e., the HOMO–LUMO transition.

## 2 Models and computational details

We combine differently sized, saturated and unsaturated nanoclusters with three anatase $TiO_2$ nanotubes having different diameters. The different systems are illustrated in Fig. 1. $(CdSe)_{13}$ and $(CdSe)_{34}$, plus the $(CdSe)_{13}$ cluster saturated with methylamine (MA) and *p*-toluidine (PTOL), $(CdSe)_{13}(MA)_6$ and $(CdSe)_{13}(PTOL)_6$, are employed. In four systems, 3-mercaptopropionic acid (MPA) acts as the linker molecule. See [27] for further details about these clusters. The anatase $TiO_2$ nanotubes employed here are the NT(0,8), NT(0,12) and NT(0,16), respectively.

The calculation of the absorption spectra in the time domain was performed using the CP2K/QUICKSTEP program [31, 32], which uses a hybrid Gaussian and plane wave basis set based on DFT. The PBE xc-functional was employed together with norm conserving Goedecker–Teter–Hutter (GTH) pseudopotentials [33–35]. A plane wave cutoff for the expansion of the density is set to 700 Ry together with a relative cutoff of 60 Ry. For all elements considered here, the short range, molecularly optimized double-ζ single-polarized basis set (m-SR-DZVP) were applied [36]. The atomic cores of Ti consist of a small-size core pseudopotential for which 12 explicit valence electrons are used. For Cd, the $4d^{10}5s^2$ valence electrons are included, for Se, S and O 6 valence electrons are included, for N 5 and for C and H, 4 and 1, respectively. In order to describe the band gap of Ti accurately, we used the DFT + $U$ methodology for the models that contain Ti [37, 38]. Deskins et al. [39, 40] determined the effective parameter $U$ to be 4.1 eV using CP2K. The geometries were optimized until the gradients were smaller than 0.01 eV/Å, and the cutoff for the SCF procedure was set to $\varepsilon = 10^{-7}$ Ry. Periodic boundary conditions are set in all three dimensions. The simulation cell is aligned in order to get the tube axis along the $x$-axis, and the $y$-and $z$-dimensions of the cell were set as such that the periodic images are separated by at least 10.0 Å.

The absorption spectra were calculated using the RT-TDDFT methodology as it was presented by Chen et al. [41] and as it is implemented in CP2K. Despite the periodic nature of the calculations, the procedure does not differ from that presented earlier [27, 42]. Shortly, this method consists in applying an ultrashort electromagnetic pulse on the ground-state electronic wave function. We monitored the propagation of the perturbed wave function, and the dipole moment for each time step is calculated. Through a Fourier transformation of the induced dipole moment, we obtain the absorption cross section. Chen et al. [41] proposed a stepwise electric field pulse with a duration of 12.1 as and

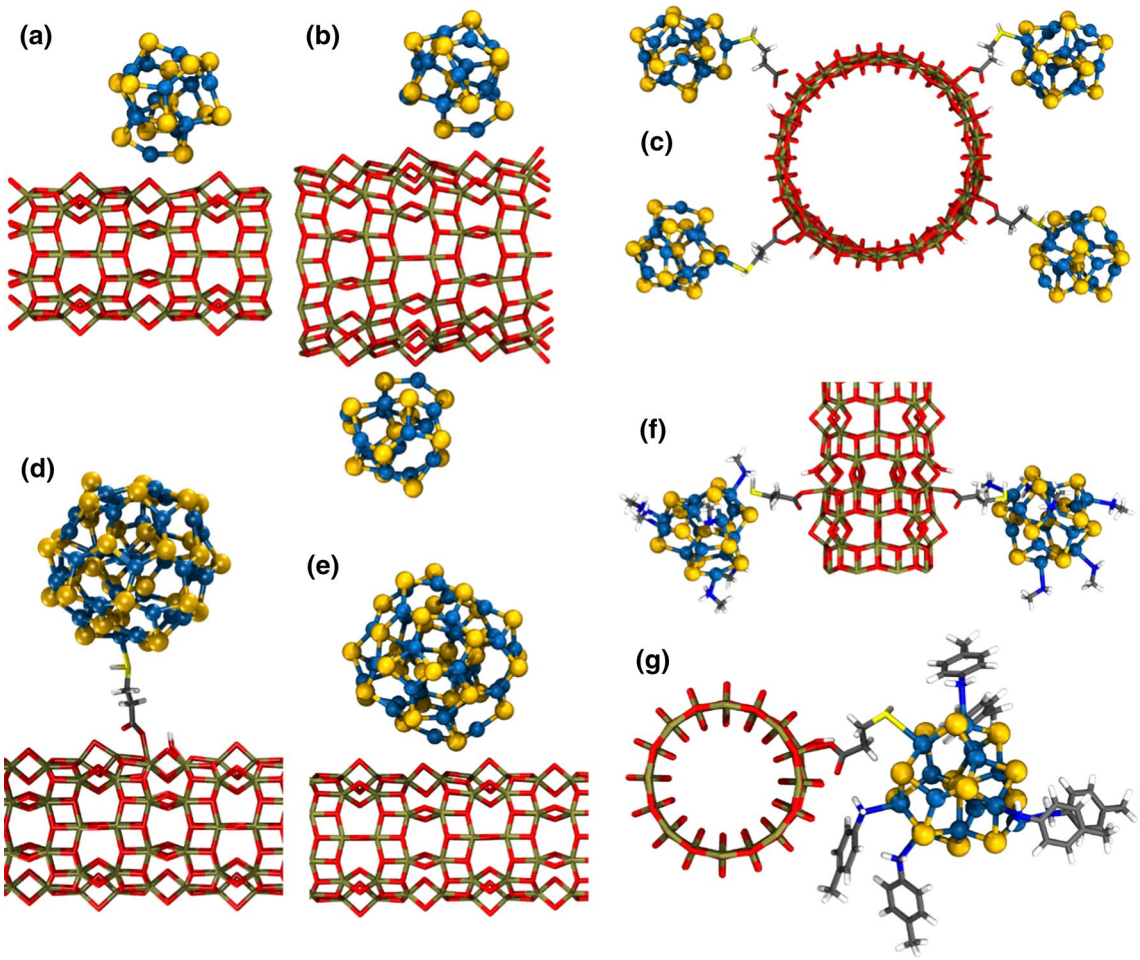


**Fig. 1** Represented are the seven systems employed throughout this work. **a** $(CdSe)_{13}$–NT(0,8), **b** $[(CdSe)_{13}]_2$–NT(0,12), **c** $[(CdSe)_{13}$–$MPA]_4$–NT(0,16), **d** $(CdSe)_{34}$–MPA–NT(0,8), **e** $(CdSe)_{34}$–NT(0,8), **f** $[(CdSe)_{13}MA_6$–MPA]2–NT(0,8), **g** $(CdSe)_{13}PTOL_6$–MPA–NT(0,8). See text for further details

a magnitude of 0.5 V/Å to perturb the wave functions. The excited wave function was propagated during 4000 steps, using the ETRS propagator [43], with a time step of 12.1 as (half the time unit in atomic units.

## 3 Results

We first present the results obtained for the bare $(CdSe)_{13}$ cluster attached directly to the small- and medium-sized nanotubes, $(CdSe)_{13}$–NT(0,8) and $[(CdSe)_{13}]_2$–NT(0,12). In Table 1, the band gap of the bare cluster (2.32 eV) and that of both adsorbed clusters (1.62 eV) differ substantially. We identify the reason for this in Fig. 2. There, the projected densities of states (PDOS) for the involved atomic orbitals for the $(CdSe)_{13}$–NT(0,8) system are shown in Fig. 2a, b. The valence band (VB) edge of the $TiO_2$ nanotube is now well below the VB edge of the whole system, which is determined through the molecular orbitals located on the

**Table 1** Band gaps, $E_g$, and the first absorption peak maxima, $E_{abs}$, of the different models employed throughout this work

| System | $E_g$ | $E_{abs}$ |
|---|---|---|
| $(CdSe)^a_{13}$ | 2.32 | 2.40 |
| $(CdSe)^a_{34}$ | 1.81 | 1.86 |
| $(CdSe)_{13}(MA)^a_6$ | 2.49 | 2.58 |
| $(CdSe)_{13}(PTOL)^a_6$ | 2.35 | 2.45 |
| $(CdSe)_{13}$–NT(0,8) | 1.62 | 2.45 |
| $[(CdSe)_{13}]_2$–NT(0,12) | 1.62 | 2.45 |
| $[(CdSe)_{13}$–$MPA]_4$–NT(0,16) | 1.20 | 2.43 |
| $(CdSe)_{34}$–NT(0,8) | 1.81 | 2.02 |
| $(CdSe)_{34}$–MPA–NT(0,8) | 1.67 | 1.87 |
| $[(CdSe)_{13}(MA)_6$–$MPA]_2$–NT(0,8) | 0.71 | 2.68 |
| $(CdSe)_{13}(PTOL)_6$–MPA–NT(0,8) | 0.71 | 2.66 |

All results are given in [eV]

[a]Reference [42]

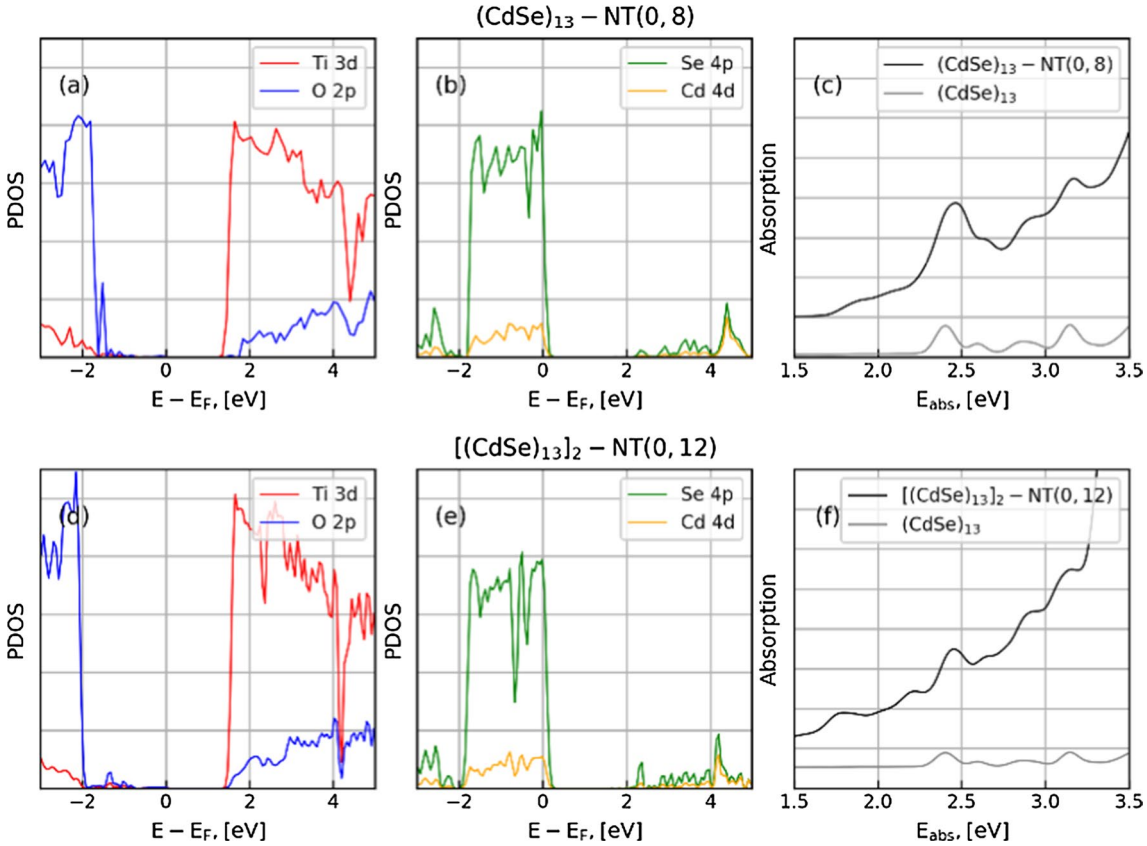


**Fig. 2** Shown are the PDOS and the absorption spectra for $(CdSe)_{13}$–NT(0,8) and $(CdSe)_{13}$–NT(0,12). **a**, **d** represent the PDOS of the nanotube part of the NT(0,8) and NT(0,12), respectively, while **b**, **e** show the QD part. The energies are shifted by the Fermi energy $E_F$. The absorption spectra for the QD–NT system together with that of the bare cluster are included in **c**, **f**

CdSe cluster. On the other side of the band gap, however, the conduction band (CB) edge constitutes mainly of the $TiO_2$ orbitals and the band gap for the QD–NT system results to be smaller compared to the separate parts of the system. Yet the impact on the spectrum, Fig. 2c is small. The first peak obtained for the $(CdSe)_{13}$ appears a 2.40 eV while after adsorption it is slightly shifted to 2.45 eV. This value is close to that reported by Liao et al. [44] for the same CdSe cluster adsorbed on a $TiO_2$ monolayer (2.34 eV). This behavior also agrees with the reported indirect type [27, 45–47] of the injection step, meaning that, first, an electron will be excited from the VB to the CB within the dot, followed by an electron transfer toward the anatase nanocluster. Since the excited electron has to overcome an energy delta of at least the size of the band gap that would correspond to that of the CdSe cluster, $E_{abs}$ is actually attributed to this QD-internal excitation.

Besides this main low energy maximum, right below 2.0 eV in Fig. 2c a small bump forms, which we attribute to the overlap between $TiO_2$ orbitals and $(CdSe)_{13}$ orbitals. The mixing between these orbitals is best observed in Fig. 2d. Above the highest contribution (− 2.0 eV) from $TiO_2$ to the MOs, small peaks form that indicate this mixing. Figure 3 depicts this graphically. In Fig. 3a, the HOMO of the QD that adsorbs directly to the nanotube extends over the tube as well, while in Fig. 3b the HOMO stays localized on the QD only. Due to this overlap, the nanotube is partially involved in the excitation and the above-mentioned absorption features appear. Next, in Fig. 2d–f we present the respective data for the $[(CdSe)_{13}]_2$–NT(0,12) system. The absorption spectrum, Fig. 2f, does not differ substantially, in particular, the first absorption peak maximum (attributed to the excitation within the quantum dot) coincides with that obtained using the NT(0,8) $TiO_2$ model, indicating that such changes in the curvature of the surface does not affect the electronic properties of the adsorbed CdSe nanocluster. This is in contrast with the more significant dependence on the surface orientation that has been observed for rutile $TiO_2$ [48]. Changing the diameter of the NT, only the features below the first absorption peak maximum, are stronger than in the $(CdSe)_{13}$–NT(0,8) model. The reason is the same as just described, but here two clusters are adsorbed instead of just one and as such, the intensity of the optical features increases due to the stronger dipole moment.

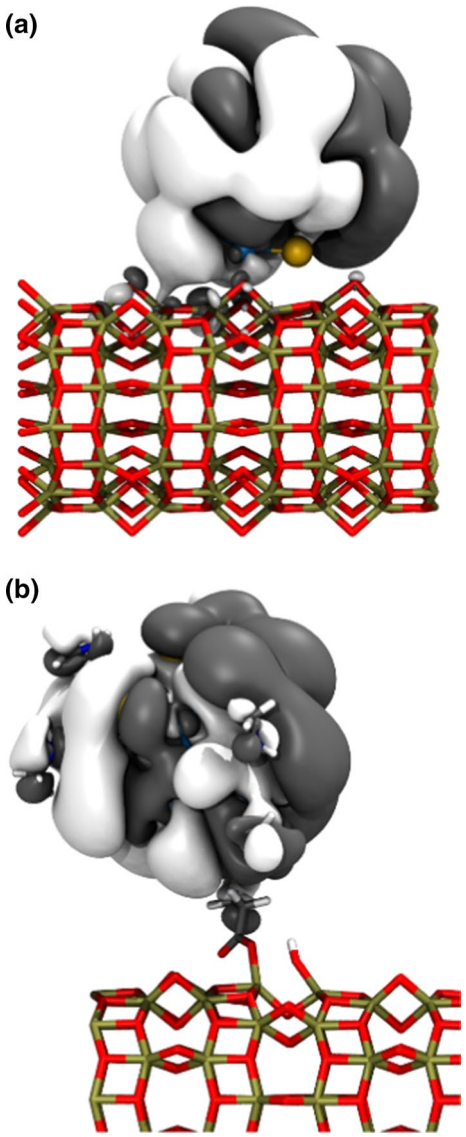


**Fig. 3** Shown are the HOMO of a directly adsorbed QD (**a**) and of a QD linked via MPA (**b**). The isovalue for the isosurfaces is set to $\pm\ 10^{-3}$ e/Bohr$^3$

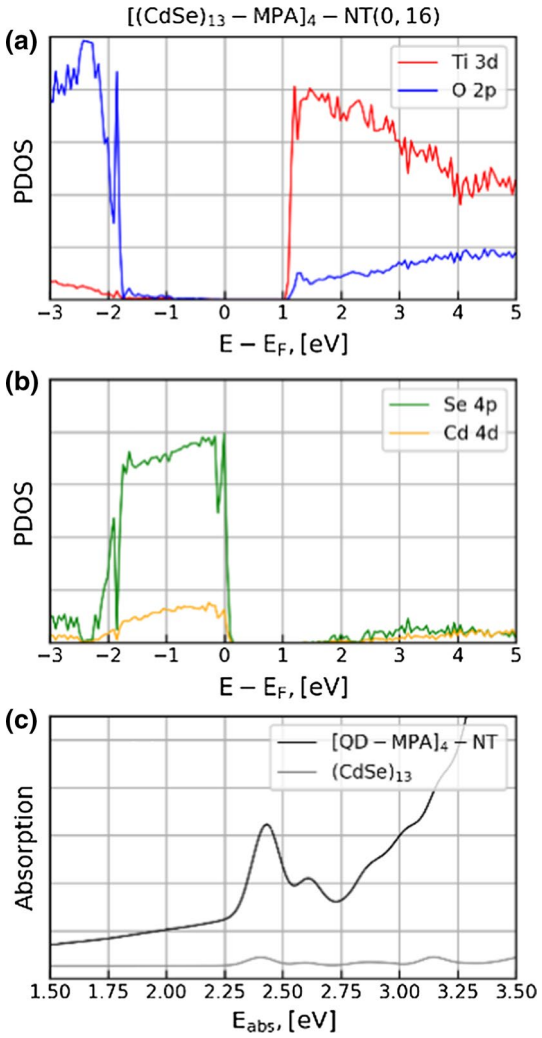


**Fig. 4** Presented are for $[(CdSe)_{13}–MPA]_4–NT(0,16)$ the partial DOS of the Ti 3*d* (red) and O 2*p* (blue) atomic orbitals in **a**, the Se 4*p* (green) and Cd 4*d* (orange) atomic orbitals in **b**. Finally, **c** contains the optical spectra of the QD–NT system (black) and of the bare $(CdSe)_{13}$ cluster (gray)

We now consider the $[(CdSe)_{13}–MPA]_4–NT(0,16)$ model, where in contrast with the $(CdSe)_{13}–NT(0,8)$ and $[(CdSe)_{13}]_2–NT(0,12)$ systems the QDs are linked via the MPA linker. From Table 1, it results that also for this model the first absorption peak maximum corresponds to that of the isolated $(CdSe)_{13}$ cluster and that it is in the same range as the other two QD–NT systems discussed above. The band gap, however, decreases by 0.42 eV from 1.62 to 1.2 eV. In Fig. 4, the different PDOS and the optical spectrum are presented. The reason for the decrease of $E_g$ is that due to the larger diameter of the nanotube its band gap decreases. Consequently, the CB edge of the $TiO_2$ anatase nanotube lowers and the gap in the whole system becomes smaller, too. The most important difference between the directly adsorbed QDs and those linked via the MPA linker, however, occurs in the absorption spectrum in Fig. 4c. Below the first absorption peak maximum at 2.43 eV, no other absorption features appear. Obviously, the missing overlap between $TiO_2$ MOs and CdSe MOs leads to a much cleaner spectrum. In summary, for the small $(CdSe)_{13}$ cluster we do not find any appreciable influence of the tube diameter on the first absorption peak maximum, although the adsorption mode (direct adsorption or linked via MPA) does have an impact on the spectrum inasmuch linked adsorption inhibits the presence of lower energy features.

Let us now investigate the effect of a larger QD on the spectrum. To do so, we replace the $(CdSe)_{13}$ QD with the larger $(CdSe)_{34}$ nanoparticle and add it to the NT(0,8) tube both via direct adsorption and linking it through the

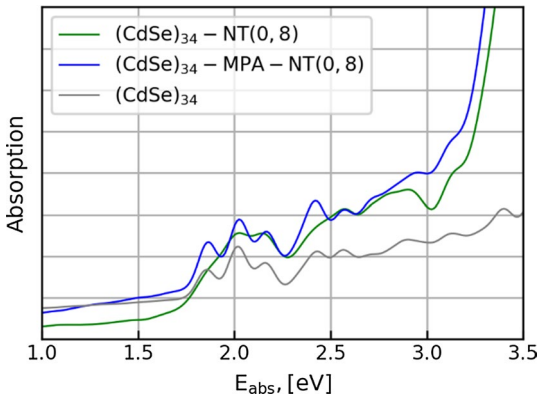


**Fig. 5** Illustrated are the optical absorption spectra of $(CdSe)_{34}$–NT(0,8) (green) and $(CdSe)_{34}$–MPA–NT(0,8) (blue). Also the spectrum of the bare $(CdSe)_{34}$ cluster (gray) is included

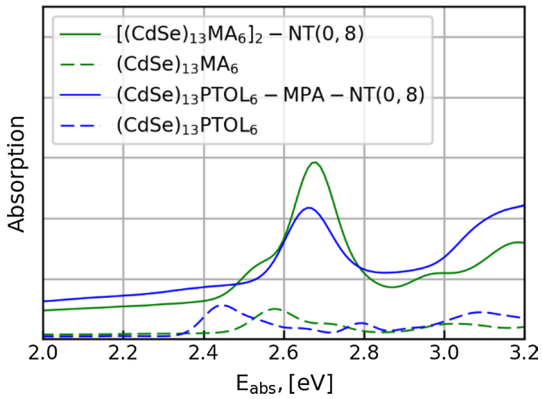


**Fig. 6** Shown are the optical absorption spectra of $[(CdSe)_{13}(MA)_6$–$MPA]_2$–NT(0,8) (green, solid line) and $(CdSe)_{13}(PTOL)_6$–MPA–NT(0,8) (blue, solid line). Also, the spectra of the corresponding isolated clusters, $(CdSe)_{13}MA_6$ (green, dashed line) and $(CdSe)_{13}PTOL_6$ (blue, dashed line), are included

MPA linker. The two models are $(CdSe)_{34}$–NT(0,8) and $(CdSe)_{34}$–MPA–NT(0,8). The spectra of these models plus the corresponding single QD are shown in Fig. 5. Table 1 suggests that upon linkage of the cluster through MPA the first absorption peak maximum decreases by 0.15 eV. Looking at the spectra in Fig. 5, the situation is not that clear. The directly adsorbed QD indeed has the first distinct absorption peak maximum at 2.02 eV (green line). But, in comparison with the spectrum of the MPA-linked QD (blue line), the typical absorption features of the $(CdSe)_{34}$ cluster (gray line) that appear in the $(CdSe)_{34}$–NT(0,8) spectrum got ironed out emerging now as a poorly resolved shoulder.

Finally, we present the results for $(CdSe)_{13}$ QDs saturated with the MA and PTOL ligands. The models are $[(CdSe)_{13}(MA)_6$–$MPA]_2$–NT(0,8) and $(CdSe)_{13}(PTOL)_6$–MPA–NT(0,8). Here, we have a rather different situation concerning the first absorption peak maxima, $E_{abs}$. Figure 6 reveals that upon attachment of two $(CdSe)_{13}(MA)_6$ clusters on the NT(0,8) nanotube, $E_{abs}$ increases from 2.58 to 2.68 eV. An even stronger increase occurs when $(CdSe)_{13}$ is saturated with the PTOL ligands. Here the increase is 0.21 eV, from 2.45 to 2.66 eV. We do not have an explanation for this observation. This feature, however, is paramount in the design of QDSSCs. As the nanoclusters grow in diameter, the band gap converges toward the bulk band gap. This has important implications for the systems investigated in the present work. As the band gap decreases, so does the energy of the CB edge. In the case of the two $(CdSe)_{34}$–NT(0,8) systems, the CB edge of the QD part coincides with the CB edge of the $TiO_2$ nanotube. At least from the absorption spectra, we do not find any evidence that this would be problematic for the case of an indirect excitation. Yet, it can be argued that it might have implications on properties like the open-circuit voltage of such a solar cell. In that case, to ensure that the LUMO of the QD is above that of the CB of the $TiO_2$ part to have an efficient QDSSC [49], the blue shift induced by capping ligands like PTOL would be enough to open the band gap of $(CdSe)_{34}$ again in order to have it within the CB of NT(0,8).

## 4 Conclusions

In summary, we investigated the optical absorption spectra of different quantum dots that are directly adsorbed or linked via a mercaptopropionic acid linker to differently sized $TiO_2$ anatase nanotubes. First of all, the optical spectra are analyzed using the partial density of states and we find that the excitation is of indirect type. Secondly, we find that whatever the mode of adsorption is, changing the diameter of the $TiO_2$ nanotube does not affect the position of the first maximum of the electronic absorption spectra. Furthermore, linking the QD to the nanotube with MPA ensures that its molecular orbitals will not mix with those of the $TiO_2$ nanotube. This avoids absorption features below the typical first absorption peak maximum inherent to each QD. As expected, increasing the size of the CdSe cluster gives rise to a red shift of the first maximum of the electronic spectra. Depending on the size of the QD, it could occur that the conduction band edge of the dot will lye below that of the $TiO_2$ nanotube. To avoid this, the QD cluster surface needs to be saturated with capping ligands, thereby pushing the QD's CB edge above that of the nanotube. When the ligand is aromatic, the first absorption peak maximum increases more in energy compared to the single QD with an aliphatic ligand.

**Acknowledgements** This work was funded by the Spanish Ministerio de Economía y Competitividad, Grant CTQ2015-64669-P, Junta de Andalucía, Grant P12-FQM-1595 and European FEDER.

## References


1. Kamat PV (2013) J Phys Chem Lett 4:908–918
2. Kakiage K, Aoyama Y, Yano T, Oya K, Fujisawa J, Hanaya M (2015) Chem Commun 51:15894–15897
3. Jiao S, Du J, Du Z, Long D, Jiang W, Pan Z, Li Y, Zhong X (2017) J Phys Chem Lett 8:559–564
4. Ip AH, Thon SM, Hoogland S, Voznyy O, Zhitomirsky D, Debnath R, Levina L, Rollny LR, Carey GH, Fischer A, Kemp KW, Kramer IJ, Ning Z, Labelle AJ, Chou KW, Amassian A, Sargent EH (2012) Nat Nanotechnol 7:577–582
5. Lee MM, Teuscher J, Miyasaka T, Murakami TN, Snaith HJ (2012) Science 338:643–647
6. Du J, Du Z, Hu J-S, Pan Z, Shen Q, Sun J, Long D, Dong H, Sun L, Zhong X, Wan L-J (2016) J Am Chem Soc 138:4201–4209
7. Gorer S, Hodes G (1994) J Phys Chem 98:5338
8. Switzer JA, Hodes G (2010) MRS Bull 35:743–796
9. Baker DR, Kamat PV (2009) Adv Funct Mater 19:805–811
10. Islam MA, Herman IP (2002) Appl Phys Lett 80:3823
11. Brown P, Kamat PV (2008) J Am Chem Soc 130:8890–8891
12. Mora-Seró I, Giménez S, Moehl T, Fabregat-Santiago F, Lana-Villareal T, Gómez R, Bisquert J (2008) Nanotechnology 19:424007
13. Guijarro N, Lana-Villarreal T, Mora-Seró I, Bisquert J, Gómez R (2009) J Phys Chem C 113:4208–4214
14. Tan Y, Jin S, Hamers RJ (2013) ACS Appl Mater Interfaces 5:12975–12983
15. Hines DA, Kamat PV (2013) J Phys Chem C 117:14418–14426
16. Pernik DR, Tvrdy K, Radich JG, Kamat PV (2011) J Phys Chem C 115:13511–13519
17. Yu L, Li Z, Song H (2017) J Mater Sci Mater Electron 28:2867–2876
18. O'Regan B, Grätzel M (1991) Nature 353:737–740
19. Chen C, Ling L, Li F (2017) Nanoscale Res Lett 12:4
20. Ferrari AM, Szieberth D, Zicovich-Wilson CM, Demichelis R (2010) J Phys Chem Lett 1:2854–2857
21. Li X, Liu L, Kang SZ, Mu J, Li G (2012) Catal Commun 17:136–139
22. Gao X, Li J, Gollon S, Qiu M, Guan D, Guo X, Chen J, Yuan C (2017) Phys Chem Chem Phys 19:4956–4961
23. Dong C, Li X, Qi J (2011) J Phys Chem C 115:20307–20315
24. Grandhi GK, Manna AK, Viswanatha R (2016) J Phys Chem C 120:19785–19795
25. Kilina S, Ivanov S, Tretiak S (2009) J Am Chem Soc 131:7717–7726
26. Inerbaev TM, Masunov AE, Khondaker SI, Dobrinescu A, Plamad A-V, Kawazoe Y (2009) J Chem Phys 131:044106
27. Nadler R, Sanz JF (2015) J Phys Chem A 119:1218–1227
28. Amaya JS, Plata JJ, Márquez AM, Sanz JF (2017) Phys Chem Chem Phys 19:14580–14587
29. Amaya JS, Plata JJ, Marquéz AM, Sanz JF (2017) J Phys Chem A 121:7290–7296
30. Amaya JS, Plata JJ, Márquez AM, Sanz JF (2016) Theor Chem Acc 135:70
31. The CP2K Developers Group (2000–2017). https://www.cp2k.org
32. Van de Vondele J, Krack M, Mohamed F, Parrinello M, Chassaing T, Hutter J (2005) Comput Phys Commun 167:103–128
33. Goedecker S, Teter M, Hutter J (1996) Phys Rev B 54:1703–1710
34. Hartwigsen C, Goedecker S, Hutter J (1998) Phys Rev B 58:3641–3662
35. Krack M (2005) Theor Chem Acc 114:145–152
36. VandeVondele J, Hutter J (2007) J Chem Phys 127:114105–114114
37. Dudarev SL, Manh DN, Sutton AP (1997) Philos Mag B 75:613–628
38. Dudarev SL, Botton GA, Savrasov SY, Humphreys CJ, Sutton AP (1998) Phys Rev B 57:1505–1509
39. Deskins NA, Dupuis M (2009) J Phys Chem C 113:346–358
40. Deskins NA, Rousseau R, Dupuis M (2011) J Phys Chem C 115:7562–7572
41. Chen H, McMahon JM, Ratner MA, Schatz GC (2010) J Phys Chem C 114:14384–14392
42. Nadler R, Sanz JF (2013) Theor Chem Acc 132:1342–1351
43. Castro A, Marques MAL, Rubio A (2004) J Chem Phys 121:3425–3433
44. Liao T, Sun Z, Dou SX (2017) ACS Appl Mater Interfaces 9:8255–8262
45. Sánchez-de Armas R, Oviedo López J, San-Miguel MA, Sanz JF, Ordejón P, Pruneda M (2010) J Chem Theory Comput 6:2856–2865
46. Sánchez-de Armas R, Oviedo López J, San-Miguel MA, Sanz JF (2011) J Phys Chem C 115:11293–11301
47. Sánchez-de Armas R, Oviedo López J, San-Miguel MA, Sanz JF (2011) Phys Chem Chem Phys 13:1506–1514
48. Toyoda T, Yindeesuk W, Kamiyama K, Katayama K, Kobayashi H, Hayase S, Shen Q (2016) J Phys Chem C 120:2047–2057
49. Le Bahers T, Labat F, Pauporté T, Lainé PP, Ciofini I (2011) J Am Chem Soc 133:8005–8013